MicroRNA-885-5p regulates cell cycle progression in liver cancer cells

CHAIYABOOT ARIYACHET[1,2], ARCHITTAPON NOKKEAW[1,2] and PISIT TANGKIJVANICH[1,2]

[1]Department of Biochemistry, Faculty of Medicine, Chulalongkorn University, Bangkok 10330, Thailand; [2]Department of Biochemistry, Center of Excellence in Hepatitis and Liver Cancer, Faculty of Medicine, Chulalongkorn University, Bangkok 10330, Thailand

Received March 4, 2025; Accepted July 31, 2025

DOI: 10.3892/ijmm.2025.5608

Abstract. MicroRNAs (miRNAs) are small non-coding RNAs that regulate gene expression by targeting messenger RNAs for translational repression or degradation. Dysregulation of miRNAs has been implicated in liver cancer development, including hepatocellular carcinoma (HCC). The present study identified miR-885-5p as a novel tumor-suppressor miRNA in liver cancer. Analysis of miRNA expression profiles from The Cancer Genome Atlas Program and Gene Expression Omnibus databases demonstrated a consistent downregulation of miR-885-5p in HCC tissues. Overexpression of miR-885-5p via lentiviral transduction significantly suppressed liver cancer cell proliferation, supporting its tumor-suppressive role. To investigate the underlying mechanism, transcriptomic profiling of miR-885-5p-overexpressing liver cancer cells was performed. Kyoto Encyclopedia of Genes and Genomes and Gene Ontology analyses highlighted the cell cycle as the most significantly affected pathway. Specifically, miR-885-5p downregulated key G_1/S transition-promoting genes, including *CDK6*, E2F Transcription Factor 2 and Origin Recognition Complex Subunit 1 (*ORC1*), in liver cancer cells. To examine if miR-885-5p regulates the G_1/S transition, a bromodeoxyuridine labeling assay and cell cycle analysis were performed. Corroborating the transcriptomic data, liver cancer cells with overexpressed miR-885-5p exhibited reduced bromodeoxyuridine incorporation and G_1 phase arrest. To gain further mechanistic insights, bioinformatics tools were used to predict gene targets of miR-885-5p in the G_1/S transition. Dual luciferase assays were conducted, which identified the direct interaction of miR-885-5p with the 3' untranslated regions of *CDK6* and *ORC1* messenger RNAs. Given its inhibitory effect on the G_1/S transition, the therapeutic potential of miR-885-5p was assessed. miR-885-5p overexpression sensitized liver cancer cells to the CDK4/6 inhibitors palbociclib, ribociclib and abemaciclib. The present findings collectively demonstrated that miR-885-5p induces cell cycle arrest and enhances CDK4/6 inhibitor sensitivity in liver cancer, suggesting its potential as a therapeutic target.

Correspondence to: Dr Chaiyaboot Ariyachet, Department of Biochemistry, Faculty of Medicine, Chulalongkorn University, Paettayaphat Building, 1873 Rama IV Road, Phatumwan, Bangkok 10330, Thailand
E-mail: chaiyaboot.a@chula.ac.th; cariyach@gmail.com

Key words: microRNA, microRNA-885-5p, cell cycle, liver cancer, hepatocellular carcinoma, CDK4/6 inhibitors

Introduction

Liver cancer is a significant global health challenge, with hepatocellular carcinoma (HCC) being the most common primary liver malignancy, accounting for >75% of cases (1). Liver cancer develops in the setting of chronic liver diseases, which promote the accumulation of DNA mutations and epigenetic changes along with the establishment of a tumor microenvironment (2). Patients in the early stages of liver cancer can be treated by surgical resection, radiofrequency ablation and liver transplantation, whereas those with more advanced disease, particularly HCC, receive systemic therapies that employ sorafenib or lenvatinib as first-line treatment and regorafenib, cabozantinib or ramucirumab as second-line treatment (3,4). Recently, the advent of immunotherapy has demonstrated promising results for liver cancer treatment (5). Despite these successes, current therapies are only effective or suitable for a subset of patients with liver cancer (6). Thus, advancements in the understanding of the molecular pathogenesis underlying liver cancer could provide new insights for more treatment options to combat this malignant tumor.

In the human genome, only 2% of all genes encode proteins, while the majority are transcribed into non-coding RNAs (7). MicroRNAs (miRNAs) are a class of non-coding RNAs that regulate gene expression post-transcriptionally by interacting with the 3' untranslated region (3' UTR) of target messenger RNAs (mRNAs) to induce mRNA degradation and/or translational repression (8). In recent years, numerous studies have observed dysregulation of miRNAs during the initiation and progression of various liver diseases, including liver cancer (9-11). Modulation of miRNAs has been shown to be a viable approach to treating numerous types of human cancer and other diseases, and several miRNA-based therapeutics have advanced into clinical trials (12,13). For example, the miR-122 inhibitor miravirsen has been evaluated in clinical trials for hepatitis C virus (14), whereas the miR-34a mimic MRX34 has been tested in a clinical trial for various

solid tumors, including liver and lung cancer (15). Despite these advancements, no miRNA therapeutics have yet been approved for cancer treatment. Nonetheless, a growing body of preclinical research has demonstrated the immense potential of miRNA-based therapies in various cancer types, including liver cancer (16,17). Thus, given the rapid progress of RNA therapeutic development (18,19), the present study aimed to elucidate the role of miRNAs in liver cancer biology to develop a novel miRNA-based therapy for liver cancer treatment.

The present study aimed to identify potential tumor-suppressing genes from an analysis of miRNA expression profiles of normal and HCC tissue pairs from public datasets, and thus aimed to elucidate the molecular function of miR-885-5p in liver cancer cells by the transcriptomic approach and explore its therapeutic potential for liver cancer therapy.

Materials and methods

Establishment of cell lines and miR-885-5p overexpression. Liver cancer cell lines HepG2 (cat. no. HB-8065) and SNU-449 (cat. no. CRL-2234), and the non-tumorigenic human hepatocyte cell line THLE-2 (cat. no. CRL-2706) were obtained from the American Type Culture Collection. The JHH-4 cell line (cat. no. JCRB0435) was sourced from the Japanese Collection of Research Bioresources Cell Bank. The human 293FT cell line (cat. no. R70007) was obtained from Thermo Fisher Scientific, Inc. Cell lines were authenticated by short tandem repeat analysis (Macrogen, Inc.). Cells were cultured in complete growth media containing 10% fetal bovine serum (cat. no. A5256701; Gibco; Thermo Fisher Scientific, Inc.) following the manufacturers' protocols and maintained at 37˚C in a 5% CO_2 incubator.

To generate liver cancer cells stably expressing miR-885-5p, a second lentiviral vector system was utilized comprising the packaging plasmids pMD2.G (plasmid #12259; Addgene, Inc.) and psPAX2 (plasmid #12260; Addgene, Inc.) in 293FT cells (cat. no. R70007; Invitrogen; Thermo Fisher Scientific, Inc.). The pre-miRNA sequence of miR-885-5p was amplified from human genomic DNA and cloned into an *Eco*RI/*Bam*HI-cut pLVX-EF1α-IRES-Puro vector (cat. no. 631988; Takara Bio USA, Inc.). For each 6-well plate, 3.08 μg pLVX-EF1α-pre-miR-885-5p-IRES-Puro, 3.08 μg psPAX2 and 2 μg pMD2.G were co-transfected into 293FT cells with a calcium phosphate transfection kit (cat. no. CAPHOS; Sigma-Aldrich; Merck KGaA) for 8 h at 37˚C according to the established protocol (20). Lentiviral particles were collected at 48 h post-transfection and were concentrated before being used to transduce target cells at a multiplicity of infection of 3 using a spinoculation method (800 x g, 40 min, 37˚C) (21). Following transduction, cells exhibiting stable integration were selected using puromycin (cat. no. P8833; Sigma-Aldrich; Merck KGaA) at 1-2 μg/ml until all non-transduced control cells were eliminated (typically 7-10 days). Subsequently, the cells were maintained in 0.5-1 μg/ml puromycin for further experimentation. Successful overexpression of miR-885-5p was confirmed via reverse-transcription quantitative PCR (RT-qPCR). Primer sequences used for cloning and RT-qPCR analysis are detailed in Table SI.

Assessment of cell proliferation and clonogenic survival. Cell proliferation was measured using a standard MTT assay (cat. no. M6494; Invitrogen; Thermo Fisher Scientific, Inc.). Cells were incubated with 0.5 μg/ml MTT for 1 h. The formazan crystals were dissolved in dimethyl sulfoxide (DMSO), and the absorbance was read at a wavelength of 570 nm (BioTek Synergy HTX; Agilent Technologies, Inc.). Colony formation was assessed by plating 500-2,000 cells/well of a 6-well plate and culturing for 2-3 weeks. Colonies were fixed in 100% methanol for 30 min at room temperature, stained with phosphate-buffered saline containing 0.1% crystal violet (cat. no. B21932.14; Thermo Fisher Scientific, Inc.) at room temperature for 30 min and counted for colonies comprising ≥50 cells.

mRNA and miRNA expression analysis by RT-qPCR. mRNA and miRNA fractions were both isolated from liver cancer cells using the GeneAll Hybrid-R miRNA kit (cat. no. HB3520; GeneAll Biotechnology, Co., Ltd.). Complementary DNA was synthesized from the mRNA fraction using iScript Reverse Transcription Supermix (cat. no. 1708840; Bio-Rad Laboratories, Inc.) for mRNA analysis according to the manufacturer's instructions. For miRNA analysis, complementary DNA was synthesized from the miRNA fraction using RevertAid First Strand cDNA Synthesis kit (cat. no. K1621; Thermo Fisher Scientific, Inc.) according to the previous study (22). qPCR was performed on a QuantStudio 3 Real-Time PCR System (Thermo Fisher Scientific, Inc.) with CAPITAL qPCR Green Mix HRox (cat. no. BR0501901; Biotechrabbit GmbH) under the following conditions: 95˚C for 10 min, followed by 35 cycles at 95˚C for 15 sec and 60˚C for 20 sec. Relative gene expression was calculated using the $2^{-\Delta\Delta Cq}$ method (23). *RPL19* served as the internal reference gene for mRNA analysis and *U6* served as the internal reference gene for miRNA analysis. The sequences of the primers used are listed in Table SI.

Identification of differentially expressed miRNAs from public datasets. To identify key miRNAs in HCC, the Database of Differentially Expressed MiRNAs in Human Cancers (https://www.biosino.org/dbDEMC/index) was utilized (24). The top three datasets derived from HCC tissue samples with the highest number of differentially expressed miRNAs [absolute fold change (|FC|)>1.5 and adjusted P-value <0.05] were selected. Applying this criterion, datasets EXP00409, EXP00410 and EXP00576 were chosen for further analysis. Datasets EXP00409 (comparing miRNA expression between cancerous and normal liver tissues) and EXP00410 (comparing miRNA expression between stage 1 and stage 3 HCC tumors) were obtained from The Cancer Genome Atlas (TCGA) Liver Hepatocellular Carcinoma Collection project (https://portal.gdc.cancer.gov/projects/TCGA-LIHC). Dataset EXP00576, retrieved from the GSE147889 repository, also compared miRNA expression between normal and cancerous tissues from the Gene Expression Omnibus (GEO) database (https://www.ncbi.nlm.nih.gov/geo/query/acc.cgi?acc=GSE147889). For reanalysis, miRNA expression profiles from EXP00576 were processed using the GEO2R web tool (version 3.26.8; https://www.ncbi.nlm.nih.gov/geo/geo2r/). Expression data from the TCGA Liver Hepatocellular Carcinoma Collection datasets were retrieved using the TCGAbiolinks R package (R Core Team; Posit Software, PBC). All expression values were transformed using $\log_2$(expression + 1).

Transcriptomic profiling and functional enrichment analysis. RNA-sequencing (RNA-seq) analysis was performed by Beijing Biomarker Technologies Co., Ltd. RNA quality and integrity were assessed using the Agilent Bioanalyzer 2100 system (Agilent Technologies, Inc.) to ensure suitability for sequencing. Libraries were prepared using the NEBNext Ultra RNA Library Prep Kit for Illumina® (cat. no. E7770; New England Biolabs, Inc.). The final library concentration was examined using Qubit 2.0 (Thermo Fisher Scientific, Inc.), diluted to a loading concentration of 2 nM, and sequenced in paired-end 150 bp mode on the Illumina NovaSeq 6000 platform (Illumina, Inc.).

Raw sequencing reads were filtered for quality and adapter contamination. The clean reads were then mapped to the reference genome using HISAT2 (version 2.2.1; https://daehwankimlab.github.io/hisat2/). Gene expression levels were quantified using StringTie (version 2.2.1; https://ccb.jhu.edu/software/stringtie/index.shtml). Differentially expressed genes (DEGs) between control and miR-885-5p-overexpressing JHH-4 cells were identified using DESeq (version 1.30.1; http://www.bioconductor.org/packages/release/bioc/html/DESeq.html) with a threshold of |FC|>1.5 and P<0.05.

Functional enrichment analysis of DEGs was performed using g:Profiler web tool (version e109_eg56_p17_63f6c3d4; https://biit.cs.ut.ee/gprofiler_archive3/e109_eg56_p17/gost) to identify enriched Gene Ontology (GO) terms (https://geneontology.org), Kyoto Encyclopedia of Genes and Genomes (KEGG) pathways (https://www.genome.jp/kegg/pathway.html), Reactome pathways (https://reactome.org), and WikiPathways (https://www.wikipathways.org/organisms/human.html). Statistical significance for GO and KEGG pathway enrichment was determined using a false discovery rate (FDR) <0.05 and P<0.05. Gene Set Enrichment Analysis (GSEA) was performed to identify significantly enriched biological pathways associated with DEGs. The analysis was conducted for KEGG and Reactome pathways using the clusterProfiler and ReactomePA R packages (Posit Software, PBC). Differential expression analysis results, obtained from the RNA-seq data, were used to calculate a ranking metric for each gene, computed as Ranking Metric=sign(logFC)*-$\log_{10}$(P-value). The most significant negatively enriched pathways in KEGG and Reactome were then visualized using GSEA enrichment plots.

Assessment of cell proliferation via bromodeoxyuridine incorporation. Cell proliferation was assessed by measuring bromodeoxyuridine (BrdU) incorporation. Cells were incubated with 10 μM BrdU (cat. no. ab142567; Abcam) for 30-60 min at 37˚C, fixed with 4% paraformaldehyde for 15 min at room temperature and permeabilized with 2N hydrochloric acid for 30 min at room temperature. BrdU incorporation was detected by immunofluorescence using an anti-BrdU antibody (1:200; cat. no. sc-32323; Santa Cruz Biotechnology, Inc.) overnight at 4˚C, followed by Alexa Fluor 488-conjugated secondary antibody (1:500; cat. no. A-21202; Invitrogen) for 1 h at room temperature and DAPI staining (1 μg/ml; cat. no. D9542; Sigma-Aldrich; Merck KGaA) for 10 min at room temperature. Images were captured using an EVOS M7000 cell imaging system (Invitrogen; Thermo Fisher Scientific, Inc.) and BrdU-positive cells were quantified from 10 random fields/group with >2,000 nuclei counted, using ImageJ software (version 1.54g; National Institutes of Health).

Cell cycle phase distribution by flow cytometry. To determine the cell cycle distribution, liver cancer cells were harvested and fixed in ice-cold 70% ethanol overnight. After washing with 1% fetal bovine serum in phosphate-buffered saline, cells were stained by incubation in phosphate-buffered saline containing 50 μg/ml propidium iodide (PI; cat. no. P1304MP; Thermo Fisher Scientific, Inc.) and 100 μg/ml RNase A (cat. no. EN0531; Thermo Fisher Scientific, Inc.) for 30 min at 37˚C in the dark. DNA content was then analyzed using a MACSQuant X Flow Cytometer (Miltenyi Biotec, Inc.) by detecting PI fluorescence in the PE channel. Debris was excluded using FSC-A/SSC-A gating, and doublets were removed by pulse-processing (FSC-H vs. FSC-A). The proportion of cells in each phase (G_1, S and G_2/M) was quantified using the FlowJo software (version 10.10; BD Biosciences).

Assessment of apoptosis via phosphatidylserine translocation. Apoptosis was assessed using the Apoptosis/Necrosis Assay Kit (blue, green, red; cat. no. ab176749; Abcam). Liver cancer cells were washed twice with Assay Buffer and resuspended in Assay Buffer containing 1X Apopxin Green Indicator at room temperature. Cells were incubated at room temperature for 30 min while protected from light. After incubation, cells were washed twice with Assay Buffer and replaced with fresh Assay Buffer. Apoptotic cells were visualized using the fluorescein isothiocyanate channel (Ex/Em=490/525 nm) on an EVOS M7000 cell imaging system (Invitrogen; Thermo Fisher Scientific, Inc.). Images were captured using an EVOS M7000 cell imaging system (Invitrogen; Thermo Fisher Scientific, Inc.), and quantification of Apopxin Green-positive cells was performed from 10 random fields/group with >2,000 nuclei counted, using the ImageJ software (version 1.54g; National Institutes of Health).

Validation of miR-885-5p target genes via dual luciferase reporter assay. To identify potential miRNA-mRNA interactions, TargetScan web tool (version 8.0; https://www.targetscan.org/vert_80/) was used to predict miRNA targets from a pool of downregulated DEGs involved in the G_1-to-S transition, and binding sites were further predicted using RNAhybrid web tool (version 2.1.1; https://bibiserv.cebitec.uni-bielefeld.de/rnahybrid/). Based on these analyses four genes (*CDK6*, *ORC1*, *E2F1* and *E2F2*) were selected for experimental validation using a dual luciferase reporter assay. The 3' UTRs of these genes containing either wild-type (WT) or mutated (MT) binding sites were cloned into the pmirGLO vector (cat. no. E133A; Promega Corporation). The pmirGLO vector with no insert was used as the negative control. The pre-miRNA sequence of miR-885-5p was cloned into the pSilencer 3.0 H1 vector (cat. no. AM7210; Thermo Fisher Scientific, Inc.). Human 293FT cells (cat. no. R70007; Invitrogen; Thermo Fisher Scientific, Inc.) were co-transfected with these constructs by a standard calcium phosphate transfection (20). Luciferase activity was measured using the Dual-Luciferase Reporter Assay System (cat. no. E1910; Promega Corporation) 48 h post-transfection using a BioTek Synergy HTX Multi-Mode Microplate Reader

(BioTek; Agilent Technologies, Inc.). Firefly luciferase activity was normalized to *Renilla* luciferase activity for data analysis. Primer sequences used for cloning are detailed in Table SI.

Determination of protein expression by western blot analysis. Protein extracts from liver cancer cells were prepared using radioimmunoprecipitation assay lysis buffer supplemented with a protease inhibitor cocktail (cat. no. 04693132001; Roche Diagnostics). Protein concentrations were then determined using a Bradford protein assay (cat. no. 5000001; Bio-Rad Laboratories, Inc.). Equal amounts of protein (40 μg) were denatured and separated by 12% sodium dodecyl sulfate polyacrylamide gel electrophoresis. Proteins were then transferred to a nitrocellulose membrane using a semidry method (Bio-Rad Laboratories). Following transfer, membranes were blocked for 30 min in a blocking buffer (cat. no. BM01-500; Visual Protein; Energenesis Biomedical, Co., Ltd.). Membranes were subsequently incubated overnight at 4˚C with the following primary antibodies: CDK6 (1:1,000; cat. no. sc-7961; Santa Cruz Biotechnology); Origin Recognition Complex Subunit 1 (ORC1; 1:1,000; cat. no. A14756; ABclonal Biotech Co., Ltd.) and β-actin (1:2,000; cat. no. sc-47778; Santa Cruz Biotechnology). Membranes were then incubated with HRP-conjugated goat anti-rabbit or anti-mouse IgG secondary antibody (1:5,000; cat. no. 7074 and 7076, respectively; Cell Signaling Technology) for 1 h at room temperature. Protein bands were visualized using an enhanced chemiluminescence substrate (cat. no. RPN3004; Cytiva) and imaged using a ChemiDoc Touch Imaging System (Bio-Rad Laboratories, Inc.). Densitometric quantification of protein band intensity was performed using the ImageJ software (version 1.54g; National Institutes of Health) and levels were normalized against those of β-actin as a loading control.

Determination of CDK4/6 inhibitor half-maximal inhibitory concentration values. Abemaciclib (cat. no. HY-16297A), palbociclib (cat. no. HY-50767) and ribociclib (cat. no. HY-15777B) were purchased from MedChemExpress and dissolved in DMSO to prepare stock solutions at a concentration of 20 mM. Serial dilutions were performed to achieve final drug concentrations ranging from 0 to 50 μM. The final concentration of DMSO in all treatment conditions did not exceed 0.5% (v/v), and an equivalent volume of DMSO was added to control cells to ensure consistency across experimental conditions. Cells were seeded at a density of $1x10^4$ cells/well, and drug treatments were carried out for 72 h at 37˚C in a 5% CO_2 incubator. The half-maximal inhibitory concentration (IC_{50}) of each drug was determined in both control and miR-885-5p-overexpressing cells using the MTT assay as previously mentioned. Dose-response curves were generated and IC_{50} values were calculated using non-linear regression analysis using the GraphPad Prism software (version 9; Dotmatics).

Statistical analysis. Data are presented as mean ± standard deviation. Statistical significance was determined using GraphPad Prism (version 10; Dotmatics). Unpaired, two-tailed Student's t-tests were used for comparisons between two groups. One-way analysis of variance was used for comparisons among ≥3 groups. Spearman correlation analysis was used to study the relationship between miR-885-5p and cell cycle genes in HCC tissues. Non-linear regression analysis was employed to analyze the effects of CDK4/6 inhibitors on liver cancer cells. $P<0.05$ was considered to indicate a statistically significant difference. All experiments were performed independently at least twice, with each condition tested in triplicate.

Results

miRNA-885-5p shows tumor-suppressing effects in liver cancer cells. To identify miRNAs with potential roles in liver cancer pathogenesis, miRNA expression profiles were reanalyzed from normal and HCC tissue pairs (dataset IDs. EXP00409 and EXP00576) and low-grade vs. high-grade HCC tissues (dataset ID. EXP00410) using the Database of Differentially Expressed MiRNAs in Human Cancers (24). miRNAs that were significantly downregulated in HCC or high-grade HCC were prioritized, as it was hypothesized that these miRNAs may potentially function as tumor suppressors. The analysis demonstrated five commonly downregulated miRNAs across all three datasets: miR-99a-5p, miR-122-3p, miR-122-5p, miR-139-5p, and miR-885-5p (Fig. 1A and Table SII). While the tumor-suppressive roles of several of these miRNAs are well-documented (25-29), presently, the specific function of miR-885-5p in HCC is the least known. Therefore, investigation was conducted to uncover novel mechanistic insights into its tumor-suppressive role in HCC. Supporting the present hypothesis, miR-885-5p was consistently downregulated in HCC tissues compared with normal tissues across both the TCGA (dataset EXP00409, $P=0.005$) and GEO (dataset EXP00576, $P<0.001$) datasets (Fig. 1B). Furthermore, it showed significant downregulation in high-grade tumors (dataset EXP00410, $P=0.001$). Furthermore, 5-year Kaplan-Meier survival analysis was performed on TCGA-LIHC cohort. Patients were stratified into high- and low-expression groups for miR-885-5p; the high-expression group was defined as patients with expression at or above the 80th percentile, while the low-expression group consisted of those with expression below this threshold. This analysis demonstrated that high miR-885-5p expression was associated with significantly prolonged overall survival in patients with HCC ($P=0.0204$; hazard ratio, 0.61; 95% confidence interval, 0.40-0.93; Fig. 1C).

To investigate the functional roles of miR-885-5p in HCC, the pre-miRNA sequence of miR-885-5p was cloned into a lentiviral vector and transduced into three liver cancer cell lines: HepG2, JHH-4 and SNU-449. These cell lines exhibited reduced expression levels of endogenous miR-885-5p compared with that of a normal hepatocyte cell line, THLE-2 ($P<0.001$; Fig. 1D). Cells transduced with a lentivirus containing a scrambled miRNA sequence served as controls. Following puromycin selection, successful miR-885-5p overexpression (885-OE) was confirmed by RT-qPCR. Significant miR-885-5p induction was achieved in each cell line compared with its respective control (HepG2, $P<0.001$; JHH-4, $P=0.001$; SNU-449, $P=0.002$; Fig. 1E). While the absolute levels of overexpression varied among cell lines, consistent and robust relative induction was observed. MTT assays demonstrated that 885-OE cells significantly impaired cell proliferation in all three liver cancer cell lines compared with that of control

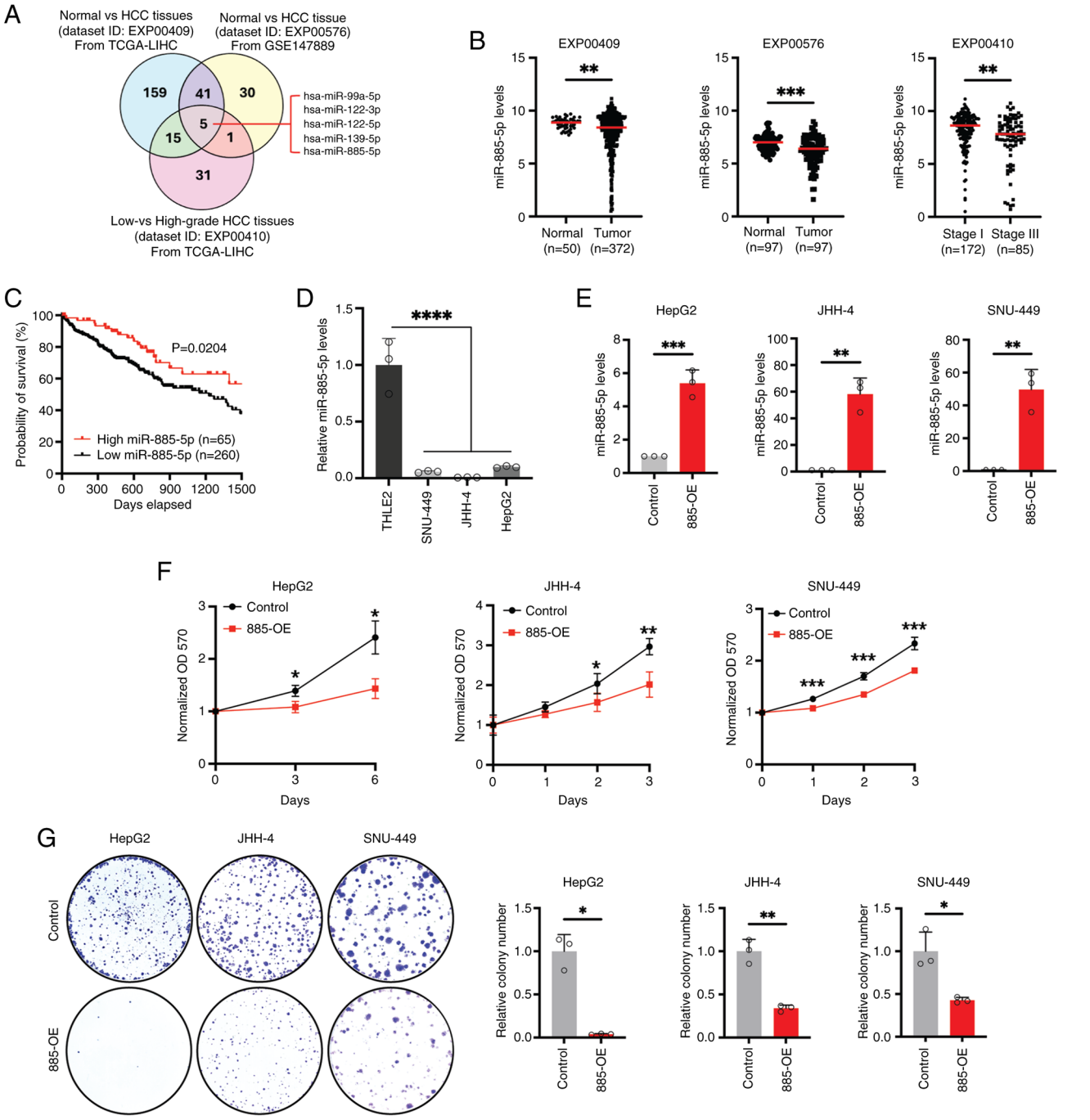

Figure 1. miR-885-5p shows tumor-suppressing effects in liver cancer cells. (A) Reanalysis of microRNA profiling from three datasets curated by the Database of Differentially Expressed MiRNAs in Human Cancers to identify downregulated miRNAs in HCC tissues. (B) Expression of miR-885-5p in normal liver tissues, low-grade and high-grade HCC tissues from Database of Differentially Expressed MiRNAs in Human Cancers datasets. Statistical significance was determined using the Mann-Whitney test for clinical data. (C) Kaplan-Meier survival analysis of patients with HCC with low and high expression of miR-885-5p from TCGA database. (D) RT-qPCR analysis of miR-885-5p in normal hepatocyte cell line (THLE-2) and liver cancer cell lines (HepG2, JHH-4 and SNU-449). Statistical significance was determined using the one-way ANOVA with Tukey's multiple comparison test. (E) RT-qPCR analysis of miR-885-5p in liver cancer cell lines with 885-OE. (F) MTT-based proliferation assays in control and 885-OE liver cancer cells. (G) Colony formation assay of control and 885-OE liver cancer cells with representative images and quantification of colony numbers/well. Data are shown as the mean ± standard deviation from $n \geq 3$ replicates from at least two independent experiments. Statistical significance was determined using Student's t-test for *in vitro* assays. *P<0.05, **P<0.01, ***P<0.001 and ****P<0.0001. miR, microRNA; HCC, hepatocellular carcinoma; 885-OE, miR-885-5p overexpressed; TCGA, The Cancer Genome Atlas; LIHC, Liver Hepatocellular Carcinoma Collection; RT-qPCR, reverse transcription-quantitative PCR.

cells (HepG2, P=0.01; JHH-4, P=0.002; SNU-449, P<0.001; Fig. 1F). Consistent with this defect, 885-OE cells also demonstrated reduced colony formation ability compared with that of control cells (HepG2, P=0.013; JHH-4, P=0.001; SNU-449, P=0.045; Fig. 1G).

Overexpression of miR-885-5p downregulates multiple genes involved in the G_1-to-S transition. To elucidate the molecular mechanisms underlying the tumor-suppressive function of miR-885-5p, RNA-seq on control and 885-OE JHH-4 cells (GEO ID. GSE290378) was performed. Transcriptome

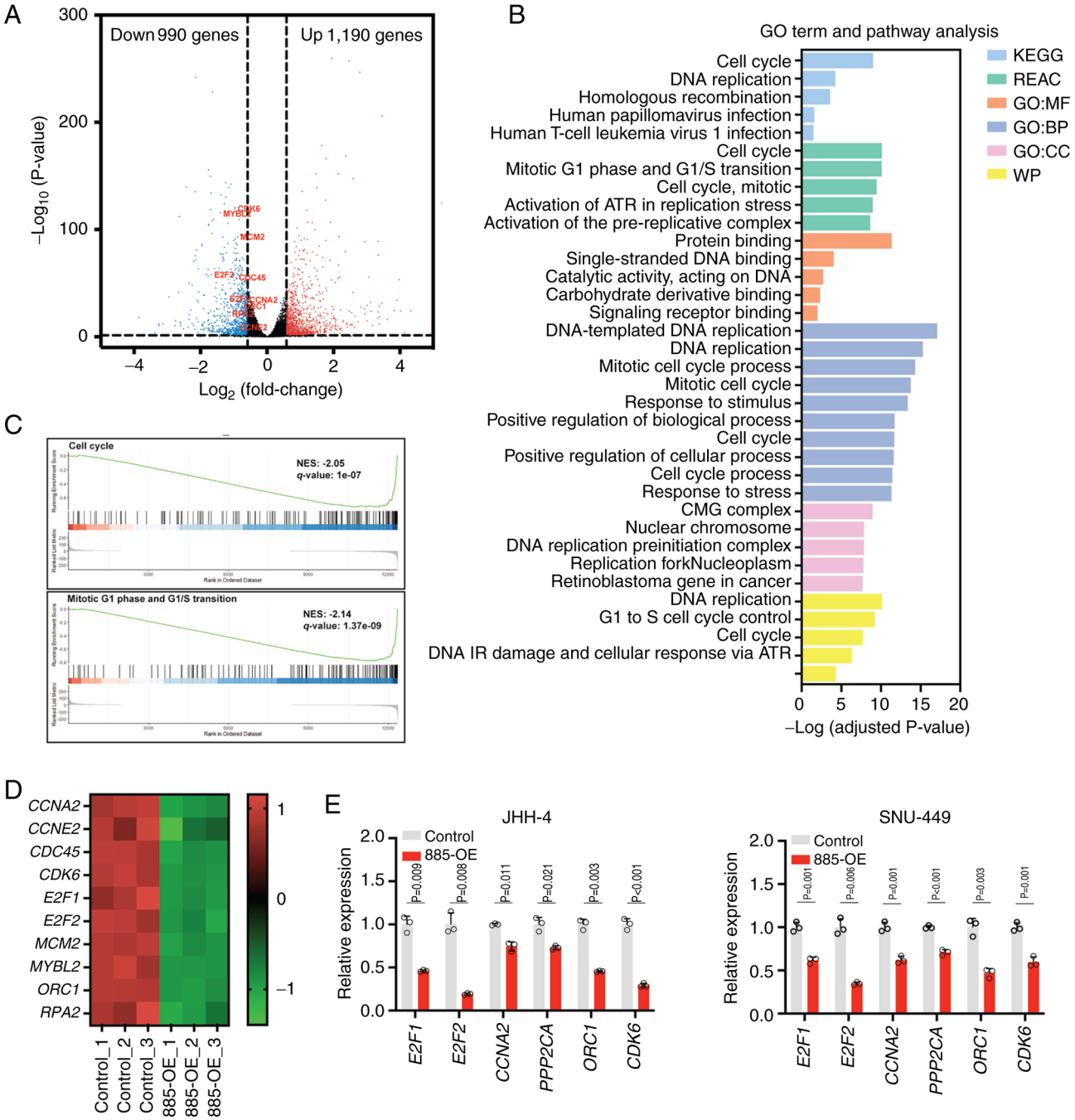

Figure 2. RNA-sequencing analysis of JHH-4 cells with miR-885-5p overexpression. (A) The volcano plot represents $\log_2$ fold change and statistical significance ($-\log_{10}$ P-value) for gene expression of control and JHH-4 cell lines with overexpression of miR-885-5p. DEGs were identified based on an absolute fold change >1.5 and P-value <0.05. Significantly upregulated and downregulated DEGs are shown as red and blue dots, respectively. (B) Overall functional enrichment analysis of downregulated DEGs using Kyoto Encyclopedia of Genes and Genomes, Reactome, Gene Ontology, and WikiPathways with an adjusted P<0.05. (C) Gene Set Enrichment Analysis identified a downregulation of DEGs involved in the cell cycle and G_1/S transition. (D) The heatmap visualized gene expression patterns of cell cycle-related genes where red and green represent upregulated and downregulated levels, respectively. (E) RT-qPCR validation of cell cycle-related genes identified in RNA-seq analysis from three replicates. RT-qPCR experiments were normalized to the control group and analyzed using Student's t-test. Data are presented as mean ± standard deviation, with significance levels. miR, microRNA; NES, Normalized enrichment score; Differentially expressed genes, DEGs; 885-OE, miR-885-5p overexpression; RT-qPCR, reverse transcription-quantitative PCR.

analysis demonstrated 1,190 upregulated and 990 downregulated DEGs in 885-OE cells compared with controls (|FC|>1.5 and P<0.05; Fig. 2A; Tables SIII and SIV). Consistent with the typical inhibitory effect of miRNAs on mRNA targets, further analysis on downregulated DEGs was conducted. KEGG analysis indicated that miR-885-5p overexpression significantly affected the cell cycle, DNA replication and homologous recombination (P<0.001; Fig. 2B). GO enrichment analysis demonstrated the G_1/S transition as a key affected process (P<0.001; Fig. 2B). Reactome and WikiPathways analyses further supported this finding, demonstrating the potential role of miR-885-5p in the G_1/S checkpoint (P<0.001; Fig. 2B). GSEA corroborated these findings, demonstrating a significant association between miR-885-5p overexpression

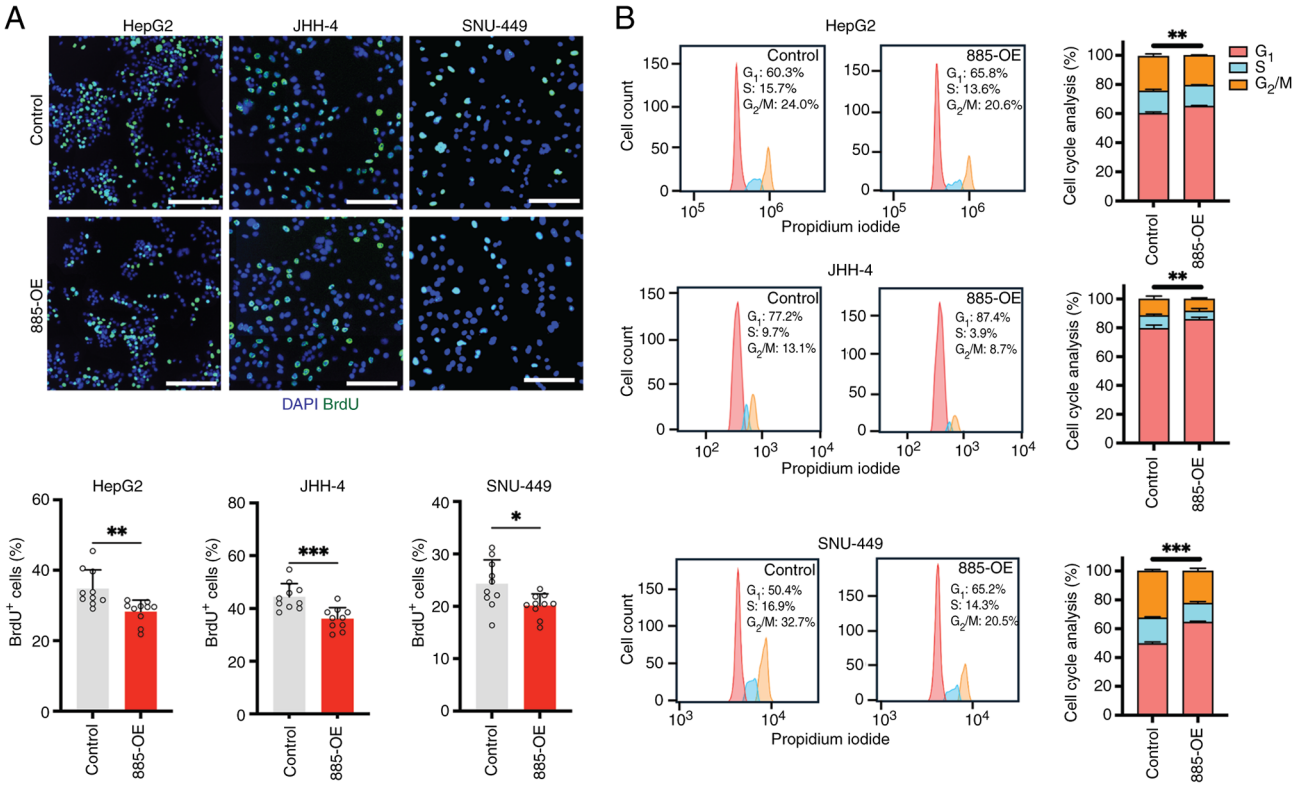

Figure 3. Overexpression of miR-885-5p promotes G_1 arrest in the cell cycle. (A) BrdU incorporation assay in control and liver cancer cell lines with overexpression of miR-885-5p with representative images and quantification of BrdU-positive cells from 10 randomly selected fields. (B) Cell cycle analysis of control and liver cancer cell lines with overexpression of miR-885-5p (n=3). All experiments were performed in three independent liver cancer lines. Fluorescent images were captured under identical exposure settings for comparison. Data are presented as mean ± standard deviation and analyzed by Student's t-test for statistical significance. *P<0.05, **P<0.01 and ***P<0.001. Scale bar, 100 μm. miR, microRNA; BrdU, Bromodeoxyuridine; DAPI, 4',6-diamidino-2-phenylindole; 885-OE, miR-885-5p overexpression.

and downregulation of key G_1/S transition genes, including *CDK6*, E2F Transcription Factor (*E2F1*), *E2F2* and *ORC1* (GSEA analysis, q<0.001; Fig. 2C and D). To validate these findings, RT-qPCR analysis was performed on a representative list of top downregulated genes involved in the G_1/S transition, including *CDK6*, *CCNA2*, *E2F1*, *E2F2*, *PPP2CA* and *ORC1* in two independent liver cancer cell lines, which confirmed their significant downregulation in 885-OE cells (Fig. 2E).

Overexpression of miR-885-5p promotes G_1 arrest in the cell cycle. The G_1/S transition, a critical checkpoint for DNA replication, is frequently dysregulated in cancer, leading to uncontrolled proliferation (30,31). To investigate if miR-885-5p regulates this transition, BrdU incorporation assays were performed. This method identifies cells in S phase and assesses G_1/S progression, where a decrease in BrdU incorporation indicates impaired transition from G_1 (gap phase 1) into S phase (DNA synthesis) (32). A significant decrease in BrdU incorporation in 885-OE cells was demonstrated, indicating a reduced proportion of cells in S phase (HepG2, P=0.004; JHH-4, P<0.001; SNU-449, P=0.019; Fig. 3A). Cell cycle analysis by flow cytometry was subsequently performed to precisely quantify the proportion of cells in each cell cycle phase (G_1, S and G_2/M). This analysis confirmed G_1 arrest in 885-OE cells, demonstrating an increased proportion of cells in the G_1 phase (HepG2, P=0.002; JHH-4, P=0.007; SNU-449, P<0.001; Fig. 3B). These findings were consistent across three liver cancer cell lines and aligned with the reduced proliferation and colony formation observed in aforementioned MTT and colony formation assays. Furthermore, the G_1 accumulation in 885-OE cells was consistent with the enrichment of pathways governing G_1/S transition identified in the present RNA-seq analysis. To further assess the impact of miR-885-5p on cell fate, its effect on apoptosis was investigated. Apoptosis, which is characterized by the translocation of phosphatidylserine to the outer plasma membrane leaflet, was measured using Apopxin Green Indicator staining. Overexpression of miR-885-5p significantly increased the proportion of apoptotic cells (HepG2, P<0.001; JHH-4, P<0.001; SNU-449, P=0.003; Fig. S1).

miR-885-5p directly targeted CDK6 and ORC1. To investigate whether miR-885-5p directly modulates genes involved in the G_1/S transition, potential miR-885-5p targets within the 3' UTRs of key genes identified from the G_1/S transition term highlighted by the present RNA-seq analysis were analyzed. The TargetScan tool was used to predict four genes as potential direct targets. *CDK6*, *ORC1*, *E2F1* and *E2F2* were prioritized for further validation and determined their lowest predicted minimum free energy of binding sites using the RNAhybrid web tool (Fig. 4A). WT and MT 3' UTR constructs were generated. To confirm the specificity of miR-885-5p binding, the 5' seed regions within the predicted binding sites of the MT constructs were engineered to abolish interaction.

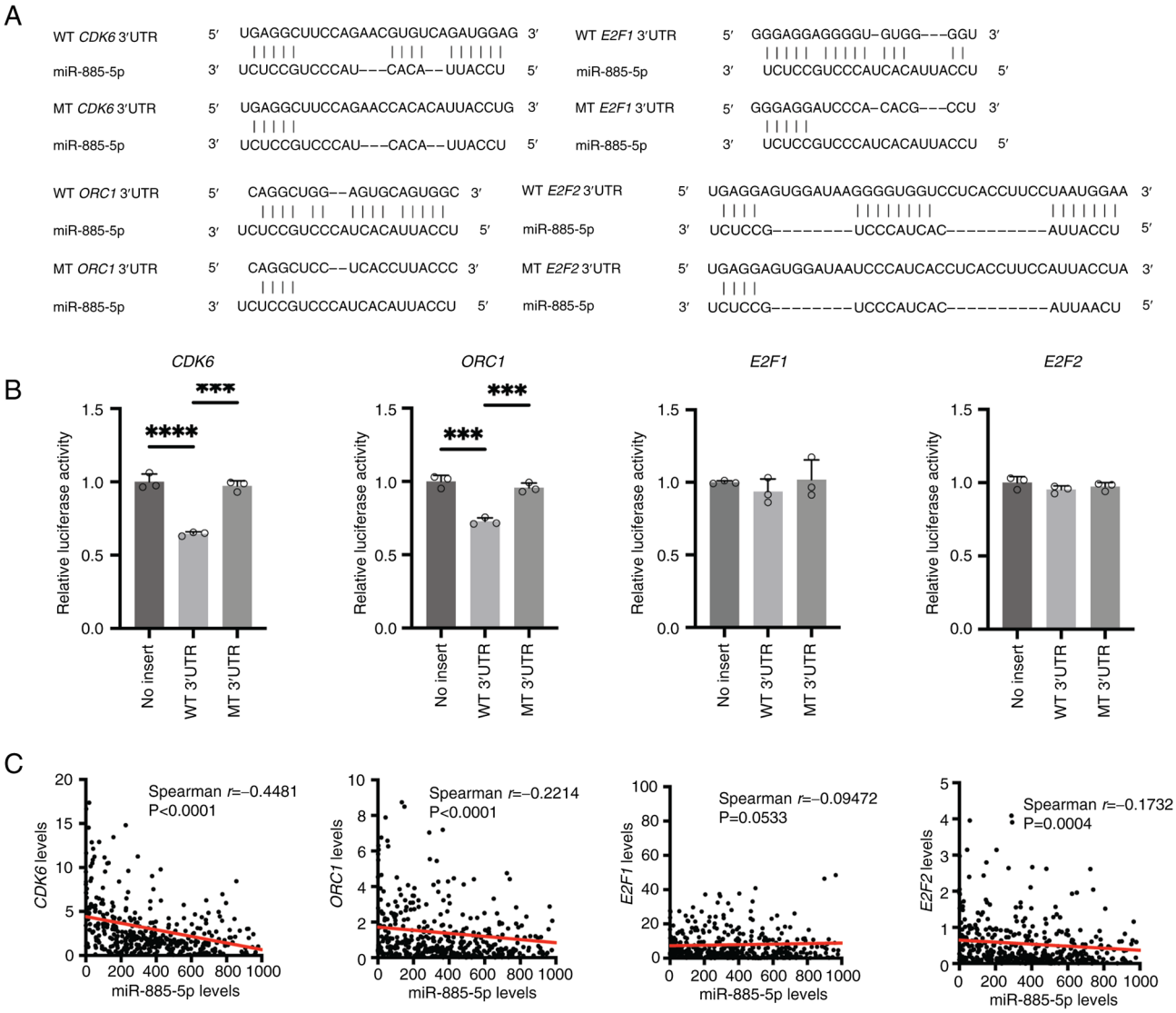

Figure 4. miR-885-5p directly regulates *CDK6* and *ORC1*. (A) Hybridization patterns predicted by the RNAhybrid tool for binding sites of miR-885-5p with WT and MT 3' UTRs of *CDK6*, *ORC1*, *E2F1* and *E2F2*. (B) Dual luciferase reporter assay for miR-885-5p and the 3' UTR of genes involved in the G_1/S transition. Relative luciferase activity was normalized to the no-insert group and analyzed using one-way ANOVA with Tukey's multiple comparison test (n=3). Data are presented as mean ± standard deviation, with significance levels indicated as ***P<0.001 and ****P<0.0001. (C) Spearman correlation (r) assessing the relationship between miR-885-5p expression (x-axis) and genes involved in the G_1/S transition (y-axis) in hepatocellular carcinoma tissue samples from The Cancer Genome Atlas database. miR, microRNA; UTR, untranslated region; WT, wild-type; MT, mutated.

Cotransfection of miR-885-5p expression plasmids with the WT constructs significantly decreased luciferase activity for the firefly luciferase reporter fused with the 3' UTRs of *CDK6* (P<0.001 vs. no-insert control) and *ORC1* (P<0.001 vs. no-insert control) but not those of *E2F1* and *E2F2* (Fig. 4B). Mutations within the miR-885-5p binding sites in the MT constructs significantly abolished this repressive effect compared with their respective WT constructs (*CDK6*, P<0.001 vs. WT; *ORC1*, P<0.001 vs. WT), thereby demonstrating the specificity of the interaction (Fig. 4B). Clinical data further supported the regulation of miR-885-5p as evidenced by a stronger negative correlation between miR-885-5p and *CDK6*/*ORC1* (*r*=-0.448 and -0.221) compared with *E2F1*/*E2F2* (*r*=-0.095 and -0.173; Fig. 4C). To validate the physiological relevance of this direct targeting, the endogenous protein expression levels of CDK6 and ORC1 upon miR-885-5p overexpression were assessed. Western blot analysis confirmed a significant downregulation of both CDK6 and ORC1 protein levels in 885-OE cells compared with control cells (P<0.001; Fig. S2).

miR-885-5p sensitizes liver cancer cells to CDK4/6 inhibitors. Given that miR-885-5p downregulated *CDK6* expression, its potential to sensitize liver cancer cells to CDK4/6 inhibitors was investigated. Drug sensitivity was quantified by IC_{50}, where lower IC_{50} values indicated increased drug sensitivity, and higher IC_{50} values indicated decreased sensitivity or resistance. Overexpression of miR-885-5p significantly increased the sensitivity of liver cancer cells to palbociclib, ribociclib and abemaciclib as demonstrated by significantly reduced IC_{50} values in the liver cancer cell lines examined (Fig. 5A-C). In SNU-449 cells, the IC_{50} for palbociclib decreased from 7.49±0.15 μM in control cells to 1.50±0.17 μM in 885-OE cells (P<0.001). In JHH-4 cells, the IC_{50} for palbociclib decreased from 8.25±1.12 μM in control cells to 3.35±0.41 μM in 885-OE

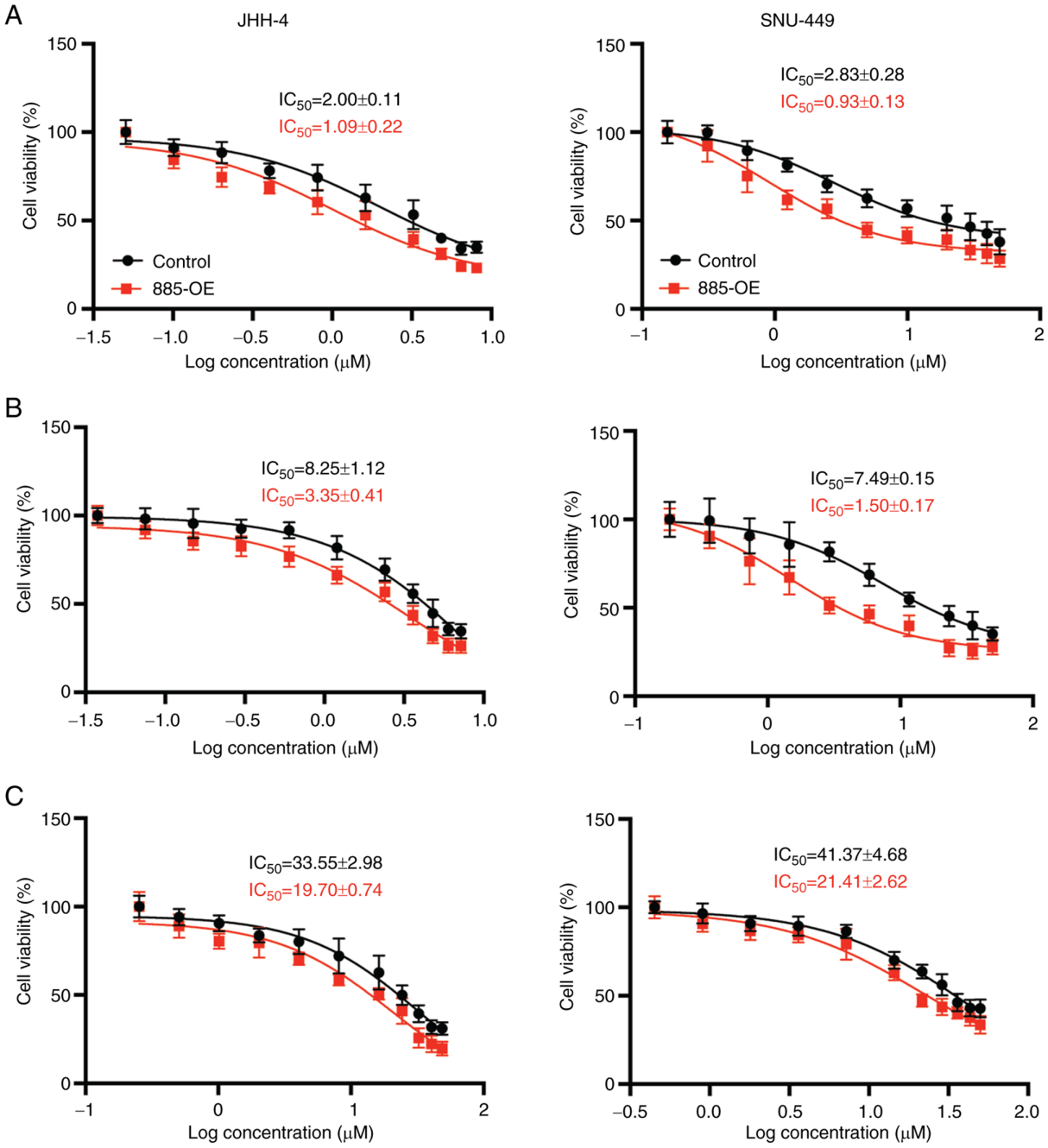

Figure 5. Overexpression of miR-885-5p sensitized liver cancer cells to CDK4/6 inhibitors. JHH-4 and SNU-449 liver cancer cells were treated with (A) abemaciclib, (B) palbociclib and (C) ribociclib with final drug concentrations ranging from 0 to 50 μM. The half-maximal inhibitory concentration of each drug was determined in both control and liver cancer cell lines with overexpression of miR-885-5p using the MTT assay. Dose-response curves were generated, and the half-maximal inhibitory concentration values were calculated using non-linear regression analysis. Each data point is presented as mean ± standard deviation from at least eight technical replicates from three independent experiments. miR, microRNA; 885-OE, miR-885-5p overexpression.

cells (P=0.028). Similar significant reductions in IC_{50} values were observed for ribociclib (SNU-449, P=0.034; JHH-4, P=0.024) and abemaciclib (SNU-449, P=0.011; JHH-4, P=0.035).

Discussion

The present study demonstrated that miR-885-5p acts as a tumor suppressor in liver cancer by modulating the G_1/S transition of the cell cycle. Significant downregulation of miR-885-5p in HCC tissues and liver cancer cells was demonstrated, while miR-885-5p overexpression inhibited cell proliferation, induced G_1 arrest and increased sensitivity to CDK4/6 inhibitors. Mechanistically, miR-885-5p directly repressed the expression of CDK6 and ORC1, two key proteins that promote S phase entry. Based on these findings, the present study proposed a model wherein miR-885-5p maintains controlled cell cycle progression in normal hepatocytes, but its suppression in liver cancer cells allows for the overexpression of cell cycle-related genes, thereby driving uncontrolled proliferation (Fig. 6). Collectively, the present data suggested that miR-885-5p may be a potential therapeutic target in liver cancer.

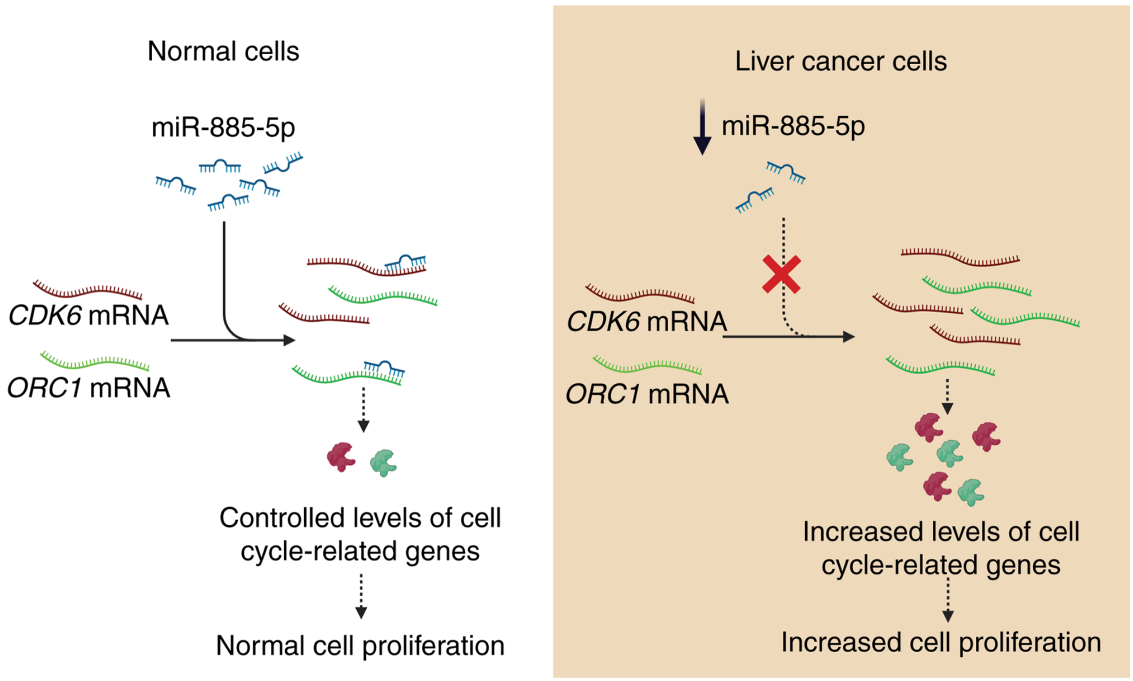

Figure 6. Proposed mechanistic model of the tumor-suppressive role of miR-885-5p in liver cancer. In normal cells (left panel), miR-885-5p is expressed at normal levels, leading to the translational repression of *CDK6* and *ORC1* mRNA. This results in controlled levels of cell cycle-related genes and normal cell proliferation. In liver cancer cells (right panel), miR-885-5p expression is downregulated, leading to the loss of translational repression of *CDK6* and *ORC1* mRNAs. Consequently, there is an increase in the levels of cell cycle-related genes, resulting in increased cell proliferation. Red and green lines represent *CDK6* and *ORC1* mRNAs, respectively. Blue lines represent miR-885-5p. The 'X' in the liver cancer cell panel represents the loss of translational repression. miR, microRNA; mRNA, messenger RNAs.

Previous studies have shown miR-885-5p as a serum biomarker for several types of cancer, including HCC (33-36). For example, Wang (34) demonstrated that low serum miR-885-5p was an independent prognostic factor for poor survival in patients with HCC, suggesting its utility as a prognostic biomarker. Similarly, other studies have evaluated its diagnostic value in other types of cancer, such as osteosarcoma, cervical cancer and clear cell renal carcinoma (33,34,36). While these studies primarily evaluated its diagnostic and prognostic value, often relying on bioinformatics to predict its targets, the present study is novel in that it investigated the functional role of miR-885-5p at a global transcriptomic level by performing RNA-seq, and analyzing the phenotypic and genotypic changes following its overexpression. This approach provided direct, data-driven insights into its novel role as a tumor suppressor. Notably, miR-885-5p has been reported to promote growth and metastasis in colorectal cancer (37) and gastric cancer (38), whereas it serves a tumor suppressor role in osteosarcoma (39) and cholangiocarcinoma (40). However, the present study demonstrated that miR-885-5p acted as a tumor suppressor in liver cancer. The contrasting roles of miR-885-5p may be attributed to tissue-specific differences in its expression and function. miRNAs can regulate different sets of target genes depending on the cellular context, leading to diverse effects on cell behavior and tumorigenesis (41). Furthermore, cancer is a heterogeneous disease, and even within the same cancer type, there can be significant variations in genetic and epigenetic profiles, tumor stage and microenvironment (42). These variations can influence the expression and function of miR-885-5p, leading to different roles in different subtypes or stages of cancer.

In the context of these varied findings, it is important to detail the reports on the functional role of miR-885-5p in liver cancer, which have also yielded diverse and sometimes contrasting findings (43-45). For example, Zhang *et al* (43) reported that miR-885-5p acts as a tumor suppressor by inhibiting HCC metastasis via the Wnt/β-catenin signaling pathway. Similarly, Xu *et al* (45) demonstrated a tumor-suppressive role, showing that miR-885-5p negatively regulates the Warburg effect by silencing hexokinase 2. Conversely, Zou *et al* (44) described an oncogenic role for miR-885-5p, suggesting it promotes liver tumorigenesis by promoting glycolysis. The findings of the present study, which suggested a tumor-suppressive role for miR-885-5p, contribute to the growing body of evidence supporting its anticancer activity in liver cancer. However, the current study is distinct in its methodology and scope. The present study employed an unbiased approach to investigate the function of miR-885-5p in liver cancer. By utilizing transcriptomic analysis (RNA-seq), the gene expression changes associated with miR-885-5p overexpression were examined, which led to identification of the novel role of miR-885-5p in regulating the G_1/S transition of the cell cycle, a critical checkpoint often dysregulated in cancer. By contrast, previous studies primarily focused on specific pathways or phenotypes, such as cancer metabolism, potentially introducing bias in their investigation of the function of miR-885-5p (43-45). The present transcriptome-wide analysis provided a broader perspective, demonstrating the impact of miR-885-5p on a fundamental process driving cell proliferation by promoting the G_1/S transition in cell cycle. This novel finding contributed to the current understanding of the tumor-suppressive

role of miR-885-5p in liver cancer and may have implications for therapeutic strategies targeting the G_1/S transition Furthermore, regarding the cell lines used in the present study, while JHH-4 and SNU-449 cells have been characterized as HCC models, reports suggest the origin of HepG2 could be either from HCC or hepatoblastoma (46,47).

The G_1/S transition stage represents a promising target for therapeutic intervention. CDK4/6 kinases serve a pivotal role in this transition, leading to the development of CDK4/6 inhibitors as anticancer agents. Although clinically approved primarily for hormone receptor-positive, HER2-negative advanced or metastatic breast cancer, these inhibitors, including palbociclib, ribociclib and abemaciclib, are also being actively studied in preclinical models for a variety of other cancer types, including non-small cell lung cancer, ovarian cancer and liver cancer (48-50). However, resistance mechanisms often emerge, highlighting the need for combination therapies to enhance their effectiveness (51). Previous studies have shown that decreasing CDK6 expression can enhance sensitivity to CDK4/6 inhibitors (52-54). The present findings demonstrated that miR-885-5p effectively downregulated CDK6, suggesting its potential to augment the antitumor activity of CDK4/6 inhibitors. The combination of miR-885-5p and CDK4/6 inhibitors represents a novel therapeutic strategy, as the synergistic potential of miR-885-5p and CDK4/6 inhibitors has not been previously explored. Notably, successful combinatorial therapies based on miRNAs and conventional drugs have been reported in preclinical models of various types of cancer, supporting the feasibility of this approach (55). For instance, in breast cancer, miR-20a-5p increases the cytotoxicity of vinorelbine, doxorubicin and paclitaxel (56); in gastric cancer, miR-129-5p augments cisplatin-induced apoptosis (57); and in liver cancer, miR-27-3p enhances the sensitivity of multidrug-resistant cells to 5-fluorouracil (58). Therefore, further investigations are warranted to explore the therapeutic potential of miR-885-5p and CDK4/6 inhibitor combinations in liver cancer.

In conclusion, the present study provided evidence for the tumor-suppressive role of miR-885-5p in liver cancer. By regulating the G_1/S transition and sensitizing liver cancer cells to CDK4/6 inhibitors, miR-885-5p represents a promising therapeutic target for liver cancer treatment. Future research should focus on validating these findings *in vivo* and exploring the clinical potential of miR-885-5p-based therapies.

Acknowledgements

Not applicable.

Funding

The present work was funded by the National Research Council of Thailand (NRCT; grant no. N42A670089), the Ratchadaphiseksomphot Fund, Graduate Affairs, Faculty of Medicine, Chulalongkorn University (grant no. GA66/077), the NSRF via the Program Management Unit for Human Resources & Institutional Development, Research and Innovation (PMU-B, grant no. B36G660010) and the Center of Excellence in Hepatitis and Liver Cancer, Faculty of Medicine, Chulalongkorn University. Further support was provided by the Second Century Fund, Chulalongkorn University and NRCT (grant no. N41A670267) for the doctoral fellowship.

Availability of data and materials

The data generated in the present study may be requested from the corresponding author. The RNA-seq data sets generated in the present study may be found in the National Center for Biotechnology Information Gene Expression Omnibus repository under the accession number GSE290378 or at the following URL: https://www.ncbi.nlm.nih.gov/geo/query/acc.cgi?acc=GSE290378.

Authors' contributions

CA and PT conceived and designed the study. AN and CA performed and analyzed the experiments. AN provided support for bioinformatic analysis. CA and PT wrote the manuscript. PT supervised the project. CA and AN confirm the authenticity of all the raw data. All authors read and approved the final version of the manuscript.

Ethics approval and consent to participate

Not applicable.

Patient consent for publication

Not applicable.

Competing interests

The authors declare that they have no competing interests.

Use of artificial intelligence tools

During the preparation of this work, AI tools (https://gemini.google.com/) were used to improve the readability and language of the manuscript, and subsequently, the authors revised and edited the content produced by the AI tools as necessary, taking full responsibility for the ultimate content of the present manuscript.

References

1. Petrick JL and McGlynn KA: The changing epidemiology of primary liver cancer. Curr Epidemiol Rep 6: 104-111, 2019.
2. Llovet JM, Kelley RK, Villanueva A, Singal AG, Pikarsky E and Roayaie S, Lencioni R, Koike K, Zucman-Rossi J and Finn RS: Hepatocellular carcinoma. Nat Rev Dis Primers 7: 6, 2021.
3. Vitale A, Trevisani F, Farinati F and Cillo U: Treatment of hepatocellular carcinoma in the precision medicine era: From treatment stage migration to therapeutic hierarchy. Hepatology 72: 2206-2218, 2020.
4. Lurje I, Czigany Z, Bednarsch J, Roderburg C, Isfort P, Neumann UP and Lurje G: Treatment strategies for hepatocellular carcinoma-a multidisciplinary approach. Int J Mol Sci 20: 1465, 2019.
5. Llovet JM, Castet F, Heikenwalder M, Maini MK, Mazzaferro V, Pinato DJ, Pikarsky E, Zhu AX and Finn RS: Immunotherapies for hepatocellular carcinoma. Nat Rev Clin Oncol 19: 151-172, 2022.
6. Yang JD and Heimbach JK: New advances in the diagnosis and management of hepatocellular carcinoma. BMJ 371: m3544, 2020.

7. ENCODE Project Consortium; Birney E, Stamatoyannopoulos JA, Dutta A, Guigó R, Gingeras TR, Margulies EH, Weng Z, Snyder M, Dermitzakis ET, *et al*: Identification and analysis of functional elements in 1% of the human genome by the ENCODE pilot project. Nature 447: 799-816, 2007.
8. Bushati N and Cohen SM: microRNA functions. Annu Rev Cell Dev Biol 23: 175-205, 2007.
9. Ma N, Tan J, Chen Y, Yang L, Li M and He Y: MicroRNAs in metabolic dysfunction-associated diseases: Pathogenesis and therapeutic opportunities. FASEB J 38: e70038, 2024.
10. Mansour RM, Abdel Mageed SS, Abulsoud AI, Sayed GA, Lutfy RH, Awad FA, Sadek MM, Shaker AAS, Mohammed OA, Abdel-Reheim MA, *et al*: From fatty liver to fibrosis: The impact of miRNAs on NAFLD and NASH. Funct Integr Genomics 25: 30, 2025.
11. Rahdan F, Saberi A, Saraygord-Afshari N, Hadizadeh M, Fayeghi T, Ghanbari E, Dianat-Moghadam H and Alizadeh E: Deciphering the multifaceted role of microRNAs in hepatocellular carcinoma: Integrating literature review and bioinformatics analysis for therapeutic insights. Heliyon 10: e39489, 2024.
12. Rupaimoole R and Slack FJ: MicroRNA therapeutics: Towards a new era for the management of cancer and other diseases. Nat Rev Drug Discov 16: 203-222, 2017.
13. Diener C, Keller A and Meese E: Emerging concepts of miRNA therapeutics: From cells to clinic. Trends Genet 38: 613-626, 2022.
14. Janssen HLA, Reesink HW, Lawitz EJ, Zeuzem S, Rodriguez-Torres M, Patel K, van der Meer AJ, Patick AK, Chen A, Zhou Y, *et al*: Treatment of HCV infection by targeting microRNA. N Engl J Med 368: 1685-1694, 2013.
15. Hong DS, Kang YK, Borad M, Sachdev J, Ejadi S, Lim HY, Brenner AJ, Park K, Lee JL, Kim TY, *et al*: Phase 1 study of MRX34, a liposomal miR-34a mimic, in patients with advanced solid tumours. Br J Cancer 122: 1630-1637, 2020.
16. Martino MT Di, Tagliaferri P and Tassone P: MicroRNA in cancer therapy: Breakthroughs and challenges in early clinical applications. J Exp Clin Cancer Res 44: 126, 2025.
17. Sareen G, Mohan M, Mannan A, Dua K and Singh TG: A new era of cancer immunotherapy: Vaccines and miRNAs. Cancer Immunol Immunother 74: 163, 2025.
18. Wang F, Zuroske T and Watts JK: RNA therapeutics on the rise. Nat Rev Drug Discov 19: 441-442, 2020.
19. Damase TR, Sukhovershin R, Boada C, Taraballi F, Pettigrew RI and Cooke JP: The limitless future of RNA therapeutics. Front Bioeng Biotechnol 9: 628137, 2021.
20. Kingston RE, Chen CA and Rose JK: Calcium phosphate transfection. Curr Protoc Mol Biol 63: 9.1.1-9.1.11, 2003.
21. Anastasov N, Höfig I, Mall S, Krackhardt AM and Thirion C: Optimized lentiviral transduction protocols by use of a poloxamer enhancer, spinoculation, and scFv-antibody fusions to VSV-G. In: Lentiviral Vectors and Exosomes as Gene and Protein Delivery Tools. Federico M (ed). Springer New York, New York, NY, pp49-61, 2016.
22. Mei Q, Li X, Meng Y, Wu Z, Guo M, Zhao Y, Fu X and Han W: A facile and specific assay for quantifying microRNA by an optimized RT-qPCR approach. PLoS One 7: e46890, 2012.
23. Livak KJ and Schmittgen TD: Analysis of relative gene expression data using real-time quantitative PCR and the 2(-Delta Delta C(T)) method. Methods 25: 402-408, 2001.
24. Xu F, Wang Y, Ling Y, Zhou C, Wang H, Teschendorff AE, Zhao Y, Zhao H, He Y, Zhang G and Yang Z: dbDEMC 3.0: Functional exploration of differentially expressed miRNAs in cancers of human and model organisms. Genomics Proteomics Bioinformatics 20: 446-454, 2022.
25. Li D, Liu X, Lin L, Hou J, Li N, Wang C, Wang P, Zhang Q, Zhang P, Zhou W, *et al*: MicroRNA-99a inhibits hepatocellular carcinoma growth and correlates with prognosis of patients with hepatocellular carcinoma. J Biol Chem 286: 36677-36685, 2011.
26. Lin CJF, Gong HY, Tseng HC, Wang WL and Wu JL: miR-122 targets an anti-apoptotic gene, Bcl-w, in human hepatocellular carcinoma cell lines. Biochem Biophys Res Commun 375: 315-320, 2008.
27. Nakao K, Miyaaki H and Ichikawa T: Antitumor function of microRNA-122 against hepatocellular carcinoma. J Gastroenterol 49: 589-593, 2014.
28. Zhang J, Jin H, Liu H, Lv S, Wang B, Wang R, Liu H, Ding M, Yang Y, Li L, *et al*: MiRNA-99a directly regulates AGO2 through translational repression in hepatocellular carcinoma. Oncogenesis 3: e97, 2014.
29. Wang K, Jiang X, Jiang Y, Liu J, Du Y, Zhang Z, Li Y, Zhao X, Li J and Zhang R: EZH2-H3K27me3-mediated silencing of mir-139-5p inhibits cellular senescence in hepatocellular carcinoma by activating TOP2A. J Exp Clin Cancer Res 42: 320, 2023.
30. Nurse P, Masui Y and Hartwell L: Understanding the cell cycle. Nat Med 4: 1103-1106, 1998.
31. Kastan MB and Bartek J: Cell-cycle checkpoints and cancer. Nature 432: 316-323, 2004.
32. Yu J, Wang Z and Wang Y: BrdU incorporation assay to analyze the entry into S phase. In: Cell-Cycle Synchronization: Methods and Protocols. Wang Z (ed). Springer US, New York, NY, pp209-226, 2022.
33. Yu F, Wang Z, Wang X, Wang S, Li X, Huang Q and Lin JH: MicroRNA-885-5p promotes osteosarcoma proliferation and migration by downregulation of cell division cycle protein 73 homolog expression. Oncol Lett 17: 1565-1572, 2019.
34. Zu Y, Wang Q and Wang H: Identification of miR-885-5p as a tumor biomarker: Regulation of cellular function in cervical cancer. Gynecol Obstet Invest 86: 525-532, 2021.
35. Wang K: Serum miR-885-5p can be used as a marker for efficacy prediction and prognosis of advanced liver cancer. Cell Mol Biol (Noisy-le-grand) 66: 135-141, 2020.
36. Liu S, Deng X and Zhang J: Identification of dysregulated serum miR-508-3p and miR-885-5p as potential diagnostic biomarkers of clear cell renal carcinoma. Mol Med Rep 20: 5075-5083, 2019.
37. Lam CSC, Ng L, Chow AKM, Wan TMH, Yau S, Cheng NSM, Wong SKM, Man JHW, Lo OSH, Foo DCC, *et al*: Identification of microRNA 885-5p as a novel regulator of tumor metastasis by targeting CPEB2 in colorectal cancer. Oncotarget 8: 26858-26870, 2017.
38. Li S, Sun MY and Su X: MiR-885-5p promotes gastric cancer proliferation and invasion through regulating YPEL1. Eur Rev Med Pharmacol Sci 23: 7913-799, 2019.
39. Liu Y, Bao Z, Tian W and Huang G: miR-885-5p suppresses osteosarcoma proliferation, migration and invasion through regulation of β-catenin. Oncol Lett 17: 1996-2004, 2019.
40. Lixin S, Wei S, Haibin S, Qingfu L and Tiemin P: miR-885-5p inhibits proliferation and metastasis by targeting IGF2BP1 and GALNT3 in human intrahepatic cholangiocarcinoma. Mol Carcinog 59: 1371-1381, 2020.
41. Suzuki HI, Katsura A, Matsuyama H and Miyazono K: MicroRNA regulons in tumor microenvironment. Oncogene 34: 3085-3094, 2015.
42. Marusyk A, Almendro V and Polyak K: Intra-tumour heterogeneity: A looking glass for cancer? Nat Rev Cancer 12: 323-334, 2012.
43. Zhang Z, Yin J, Yang J, Shen W, Zhang C, Mou W, Luo J, Yan H, Sun P, Luo Y, *et al*: miR-885-5p suppresses hepatocellular carcinoma metastasis and inhibits Wnt/β-catenin signaling pathway. Oncotarget 7: 75038-75051, 2016.
44. Zou S, Rao Y and Chen W: miR-885-5p plays an accomplice role in liver cancer by instigating TIGAR expression via targeting its promoter. Biotechnol Appl Biochem 66: 763-771, 2019.
45. Xu F, Yan JJ, Gan Y, Chang Y, Wang HL, He XX and Zhao Q: miR-885-5p negatively regulates warburg effect by silencing hexokinase 2 in liver cancer. Mol Ther Nucleic Acids 18: 308-319, 2019.
46. Knowles BB, Howe CC and Aden DP: Human hepatocellular carcinoma cell lines secrete the major plasma proteins and hepatitis B surface antigen. Science 209: 497-499, 1980.
47. López-Terrada D, Cheung SW, Finegold MJ and Knowles BB: Hep G2 is a hepatoblastoma-derived cell line. Hum Pathol 40: 1512-1515, 2009.
48. Bollard J, Miguela V, Ruiz de Galarreta M, Venkatesh A, Bian CB, Roberto MP, Tovar V, Sia D, Molina-Sánchez P, Nguyen CB, *et al*: Palbociclib (PD-0332991), a selective CDK4/6 inhibitor, restricts tumour growth in preclinical models of hepatocellular carcinoma. Gut 66: 1286-1296, 2017.
49. Zhang QF, Li J, Jiang K, Wang R, Ge JL, Yang H, Liu SJ, Jia LT, Wang L and Chen BL: CDK4/6 inhibition promotes immune infiltration in ovarian cancer and synergizes with PD-1 blockade in a B cell-dependent manner. Theranostics 10: 10619-10633, 2020.
50. Naz S, Sowers A, Choudhuri R, Wissler M, Gamson J, Mathias A, Cook JA and Mitchell JB: Abemaciclib, a selective CDK4/6 inhibitor, enhances the radiosensitivity of non-small cell lung cancer in vitro and in vivo. Clin Cancer Res 24: 3994-4005, 2018.
51. Huang J, Zheng L, Sun Z and Li J: CDK4/6 inhibitor resistance mechanisms and treatment strategies (review). Int J Mol Med 50: 128, 2022.

52. Cornell L, Wander SA, Visal T, Wagle N and Shapiro GI: MicroRNA-mediated suppression of the TGF-β pathway confers transmissible and reversible CDK4/6 inhibitor resistance. Cell Rep 26: 2667-2680.e7, 2019.
53. Yang C, Li Z, Bhatt T, Dickler M, Giri D, Scaltriti M, Baselga J, Rosen N and Chandarlapaty S: Acquired CDK6 amplification promotes breast cancer resistance to CDK4/6 inhibitors and loss of ER signaling and dependence. Oncogene 36: 2255-2264, 2017.
54. Wu X, Yang X, Xiong Y, Li R, Ito T, Ahmed TA, Karoulia Z, Adamopoulos C, Wang H, Wang L, *et al*: Distinct CDK6 complexes determine tumor cell response to CDK4/6 inhibitors and degraders. Nat Cancer 2: 429-443, 2021.
55. Dai X and Tan C: Combination of microRNA therapeutics with small-molecule anticancer drugs: Mechanism of action and co-delivery nanocarriers. Adv Drug Deliv Rev 81: 184-197, 2015.
56. Si W, Shen J, Du C, Chen D, Gu X, Li C, Yao M, Pan J, Cheng J, Jiang D, *et al*: A miR-20a/MAPK1/c-Myc regulatory feedback loop regulates breast carcinogenesis and chemoresistance. Cell Death Differ 25: 406-420, 2018.
57. Lu C, Shan Z, Li C and Yang L: MiR-129 regulates cisplatin-resistance in human gastric cancer cells by targeting P-gp. Biomed Pharmacother 86: 450-456, 2017.
58. Chen Z, Ma T, Huang C, Zhang L, Lv X, Xu T, Hu T and Li J: MiR-27a modulates the MDR1/P-glycoprotein expression by inhibiting FZD7/β-catenin pathway in hepatocellular carcinoma cells. Cell Signal 25: 2693-2701, 2013.